Journal of Magnetic Resonance 346 (2023) 107356

Contents lists available at ScienceDirect

Journal of Magnetic Resonance

journal homepage: www.elsevier.com/locate/jmr

X- and Q-band EPR with cryogenic amplifiers independent of sample temperature

Vidmantas Kalendra [a,b], Justinas Turčak [a], Jūras Banys [a], John J.L. Morton [c,d], Mantas Šimėnas [a,*]

[a] Faculty of Physics, Vilnius University, Sauletekio 3, LT-10257 Vilnius, Lithuania
[b] Amplify My Probe Ltd., London NW1 1NJ, UK
[c] London Centre for Nanotechnology, University College London, London WC1H 0AH, UK
[d] Dept. of Electronic & Electrical Engineering, University College London, London WC1E 7JE, UK

ARTICLE INFO

Article history:
Received 27 October 2022
Revised 3 December 2022
Accepted 4 December 2022
Available online 9 December 2022

Keywords:
EPR
Cryoprobe
LNA
Sensitivity
Noise
SNR

ABSTRACT

Inspired by the success of NMR cryoprobes, we recently reported a leap in X-band EPR sensitivity by equipping an ordinary EPR probehead with a cryogenic low-noise microwave amplifier placed closed to the sample in the same cryostat [*Šimėnas et al. J. Magn. Reson.* **322**, *106876 (2021)*]. Here, we explore, theoretically and experimentally, a more general approach, where the amplifier temperature is independent of the sample temperature. This approach brings a number of important advantages, enabling sensitivity improvement irrespective of sample temperature, as well as making it more practical to combine with ENDOR and Q-band resonators, where space in the sample cryostat is often limited. Our experimental realisation places the cryogenic preamplifier within an external closed-cycle cryostat, and we show CW and pulsed EPR and ENDOR sensitivity improvements at both X- and Q-bands with negligible dependence on sample temperature. The cryoprobe delivers signal-to-noise ratio enhancements that reduce the equivalent pulsed EPR measurement time by 16× at X-band and close to 5× at Q-band. Using the theoretical framework we discuss further improvements of this approach which could be used to achieve even greater sensitivity.

1. Introduction

Cryogenically cooled NMR cryoprobes containing cryogenic preamplifiers are frequently used to significantly enhance NMR sensitivity [1–4]. In these probeheads, the thermal noise is substantially reduced by simultaneous cooling of the NMR coils and low noise preamplifier, independently of the sample temperature. Despite several studies reporting promising EPR sensitivity improvements [5–11], signal preamplification with cryogenic microwave amplifiers has not yet been widely adopted in the EPR community mainly due to poor compatibility with commercial spectrometers, typical samples and high power pulsed EPR experiments.

Recently, we designed and tested an X-band EPR cryoprobe, which meets these criteria, by placing a cryogenic low noise amplifier (LNA) close to the sample on a commercially available EPR probehead [12]. To protect the LNA from high power microwave pulses employed in pulsed EPR, we incorporated a protection circuit consisting of a limiter and a fast microwave switch. The microwaves were guided to and from the resonator using a directional coupler, which also acted as partial suppressor of the input thermal noise at the expense of the excitation power. The probehead provided a significant voltage signal-to-noise ratio (SNR) improvement close to 10× below 10 K (100× reduction in the measurement time) already rendering some EPR experiments feasible that would otherwise have been impossible in a reasonable amount of time [13–15].

Here, we take further inspiration from the NMR cryoprobe and consider a more general approach, where the cryogenic LNA and its protection circuit is kept at a different temperature to that of the sample (for example, using a separate cryostat). This method has a number of potential advantages over our previous demonstration [12], the most significant being that the sensitivity gain is practically independent of the sample temperature. In addition, integrating an LNA together with its protection circuit in a limited space close to the resonator can pose practical challenges in typical cryostats, especially for ENDOR and Q-band probeheads. Using a separate cryostat outside the magnetic field applied to the sample also enables the use of microwave components such as ferrite circulators, which bring potential gains in sensitivity [12].

* Corresponding author.
E-mail address: mantas.simenas@ff.vu.lt (M. Šimėnas).

https://doi.org/10.1016/j.jmr.2022.107356
1090-7807/

We use the effective noise temperature formalism to discuss the feasibility of such a cryoprobe setup, which is then realised experimentally. The constructed cryoprobe is fully compatible with the commercial and homebuilt EPR spectrometers and, in addition to ordinary pulsed EPR probeheads, it can be easily used with high-Q CW, ENDOR and Q-band resonators. Our new setup shows about 4× voltage SNR improvement at X-band, while for measurements at Q-band, the enhancement is slightly above 2× with prospects for further improvement. In both cases, the obtained sensitivity gain is practically independent of the sample temperature.

2. Calculation of sensitivity improvement

First, we develop a theoretical framework for prediction of the sensitivity improvement provided by a generalized EPR cryoprobe with decoupled sample and cryogenic LNA temperatures. Fig. 1 shows a detection path of such a cryoprobe design, where the amplifier is held at low temperature T_{LNA} independent of the sample temperature T_{S}. The losses of the microwave paths and components prior and after the LNA are summarized as attenuators L_1, L_2, L_3, and L_4. The temperature of L_2 and L_3 is expected to be the same as that of the LNA, while L_4 is at room temperature. The attenuator L_1 reflects the interface connecting the resonator and the LNA part, and its temperature can vary depending on an exact design. The output of the external LNA is connected to a standard commercial EPR microwave bridge having a microwave amplifier placed at room temperature. The losses inside the bridge prior to this amplifier are summarized as L_5. The detection path of a standard EPR spectrometer is presented in Fig. 1, where we assume that the losses prior the microwave bridge correspond to $L_1 + L_4$ of the cryoprobe setup.

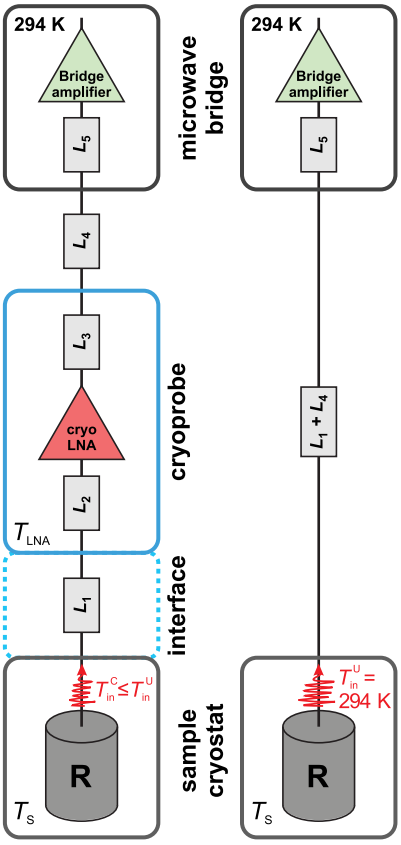

Fig. 1. Detection microwave paths of the cryoprobe (left) and standard unmodified (right) EPR setups. All lossy microwave components and cables are represented as effective attenuators $L_i (i = 1 \ldots 5)$. In the cryoprobe setup, the L_1 attenuator corresponds to an interface between the resonator (R) and the LNA circuit. In the standard setup, $L_1 + L_4$ denotes the losses between the resonator and the microwave bridge. The temperature of the sample and microwave resonator is T_{S}, while the LNA is at T_{LNA}. $T_{\mathrm{in}}^{\mathrm{C}}$ and $T_{\mathrm{in}}^{\mathrm{U}}$ denote the input noise temperatures of both setups.

The SNR improvement obtained by such a cryoprobe design compared to a standard setup can be predicted using the effective noise temperature T_{e} formalism, which was previously successfully used to calculate sensitivity of EPR setups with cryogenic LNAs [7]. The noise temperature of an LNA is typically specified by the manufacturers, while T_{e} of a passive microwave component (e.g. attenuator) depends on a physical device temperature T_{a} and can be expressed as

$$T_{\mathrm{e}} = T_{\mathrm{a}}\left(\frac{1}{G} - 1\right), \tag{1}$$

where G is the gain associated with the device. For passive lossy components, $G = 1/L$.

The total effective noise temperature of a cascaded linear microwave circuit can be expressed using the Friis equation as [16]

$$T_{\mathrm{e}} = T_1 + \frac{T_2}{G_1} + \frac{T_3}{G_1 G_2} + \frac{T_4}{G_1 G_2 G_3} + \ldots \tag{2}$$

Here, T_i and G_i correspond to the effective noise temperature and gain of an i-th device in a linear cascade, respectively.

The degradation of power SNR caused by a microwave circuit is characterized by the noise factor F defined as the ratio of the input SNR to output SNR:

$$F = \frac{\mathrm{SNR}_{\mathrm{in}}}{\mathrm{SNR}_{\mathrm{out}}}. \tag{3}$$

The noise factor can be calculated from the total effective noise temperature using

$$F = 1 + \frac{T_{\mathrm{e}}}{T_{\mathrm{in}}}, \tag{4}$$

where T_{in} denotes the noise temperature at the input of the microwave circuit.

We define the sensitivity improvement provided by the cryoprobe as the ratio of the output voltage SNR between both setups:

$$\frac{\mathrm{SNR}_{\mathrm{out}}^{\mathrm{C}}}{\mathrm{SNR}_{\mathrm{out}}^{\mathrm{U}}} = \sqrt{\frac{F^{\mathrm{C}}}{F^{\mathrm{U}}} \frac{T_{\mathrm{in}}^{\mathrm{C}}}{T_{\mathrm{in}}^{\mathrm{U}}}}, \tag{5}$$

where the subscripts C and U correspond to the cryoprobe and unmodified setups, respectively. Here, we also took into account that $\mathrm{SNR}_{\mathrm{in}} \sim 1/T_{\mathrm{in}}$. In our calculations, we take $T_{\mathrm{in}}^{\mathrm{U}} = 294$ K independent of the temperature of the sample, as in a standard setup the sample is not isolated from room temperature noise. In contrast, as demonstrated in our previous work [12], EPR cryoprobes may provide this isolation, and thus $T_{\mathrm{in}}^{\mathrm{C}}$ may be significantly lower than room temperature.

We calculated how the sensitivity improvement depends on the sample temperature T_{S} for three distinct designs derived from the generalized EPR cryoprobe. For calculations, we chose typical losses of the microwave components [12] ($L_1 = 1$ dB, $L_2 = 3$ dB, $L_3 = 1$ dB, $L_4 = 1$ dB, and $L_5 = 7$ dB), while the noise temperature of the bridge amplifier was set to 250 K. The cryogenic LNA was assumed to have typical gain (36 dB) and noise temperature (4.5 K and 50 K at 7 K and 294 K, respectively) (see below). The first design (Fig. 2b) corresponds to our previous work [12], where the LNA was placed close to the resonator meaning that $T_{\mathrm{LNA}} = T_{L_1} = T_{\mathrm{S}}$. Here, we also assume a partial suppression of the input thermal noise, which was achieved using a 6 dB directional

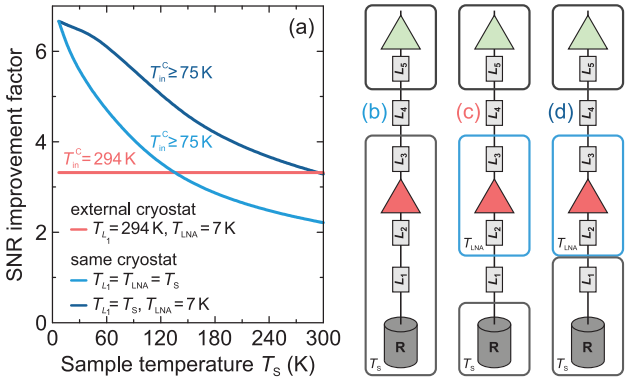

Fig. 2. (a) Sample temperature dependence of the SNR improvement provided by (b-d) three distinct EPR cryoprobe setups.

coupler, providing $T_{in}^C = 75$ K for $T_S < 75$ K, and $T_{in}^C = T_S$ for $T_S > 75$ K. The calculated behaviour of the voltage SNR improvement for this setup is presented in Fig. 2a showing a significant decay from about 6.7× to 2.2× with increasing sample temperature.

In the second design (Fig. 2c), the sample and the cryogenic LNA are kept in separate cryostats allowing to keep the temperature of the LNA fixed ($T_{LNA} = 7$ K) and independent of the sample temperature. As both cryostats are interfaced by a room temperature microwave path L_1 ($T_{L_1} = 294$ K), we assume no suppression of the input thermal noise ($T_{in}^C = 294$ K), which corresponds to the lowest bound of the sensitivity gain. This still results in a significant SNR improvement by 3.3×, which is independent of T_S (Fig. 2a). In addition, a comparison with the first design shows a crossover point at about 130 K, where the sensitivity of the external cryostat setup becomes higher.

We also explored a third design (Fig. 2d), where the sample and the LNA are kept in different regions of the same cryostat unit allowing to decouple their temperatures. Experimental realization of such a setup may be feasible in closed cycle He cryostats having a variable temperature insert (sample space), which is separated from a cold pulse tube (LNA space). In our calculations for this design, we consider that the LNA and its protection circuit are kept at $T_{LNA} = 7$ K, while the losses associated with the interface L_1 are at the sample temperature ($T_{L_1} = T_S$). We also assume the same level of suppression of the input thermal noise as for the first design ($T_{in}^C \geqslant 75$ K). Our calculations reveal that this setup would have the highest sensitivity gain with a less pronounced temperature dependence compared to the first design (Fig. 2a). However, the experimental realisation of such a cryoprobe solution is likely to require significant modifications of a closed cycle cryostat, or indeed a bespoke design.

Note, that in our analysis we ignored the resonator coupling effects on the input thermal noise [7]. A fully overcoupled resonator used in pulsed EPR should reflect the majority of input thermal noise to the detection circuit, which corresponds to the situation described in our analysis. In contrast, a critically coupled resonator employed, for example, in CW EPR would absorb all input thermal noise, and in this case T_{in}^C would match the temperature of the resonator given absence of other noise sources.

In our calculations we used typical values of microwave losses and suppression of input thermal noise. In reality, these numbers may differ resulting in different (potentially higher) sensitivity gains, although the qualitative behaviour of all three setups should remain. In the following, we demonstrate experimental implementation and testing of the second cryoprobe design for X- and Q-band EPR based on a separate cryostat for the LNA.

3. Setup details

3.1. X-band

The block diagram of our setup based on an externally cooled LNA is presented in Fig. 3a (photo of the setup is given in Figure S1). The LNA is contained in a commercially available closed-cycle He cryostat (Advanced Research Systems DE-204PE), which allows cooling and maintaining the LNA at about 7 K. The temperature of the amplifier is measured using a silicon diode temperature sensor. The cryogenic LNA is a high electron mobility transistor (HEMT) amplifier LNC4_16B from Low Noise Factory (see Table 1 for details). Our setup is simultaneously connected to a standard microwave bridge (Bruker ELEXSYS E580/IF-Q, recently confirmed to be within the expected specifications by Bruker) and EPR probehead. Depending on the experiment, we use standard Bruker ER4118X-MD5 (pulsed EPR), EN4118X-MD4 (pulsed ENDOR) and high-Q ER4102ST (CW) resonators. The temperature of the sample is independently maintained using other He cryostats (Oxford Instruments CF935 and ESR900) connected to a Stinger Cryogen-Free variable temperature system.

The microwave circuit inside the external cryostat is shown in Fig. 3b. The microwave pulses coming from the EPR bridge are directed to the EPR probehead via a three-port circulator (Table 1) placed within the external cryostat. The same circulator is used to route the microwave signals from the resonator to the LNA path, where a high-power Narda LIM-301 limiter (Table 1) protects the LNA from high power microwave pulses produced by a 1 kW traveling-wave tube (TWT) amplifier that are reflected from the resonator. A much weaker spin signal passes through the limiter and after amplification by the LNA leaves the external cryostat and travels to the EPR bridge for detection. We also tested our X-band setup using a four-port circulator with the additional port terminated by a 50 Ω load, but observed no significant differences in the performance.

In our previous study, when placing the LNA and its protection circuit directly on an EPR probehead, we employed a directional coupler instead of a circulator, as circulators degrade their properties in the magnetic field [12]. Using a circulator instead of a directional coupler is advantageous, as practically all of the spin signal is directed to the LNA path, which is in contrast to a directional cou-

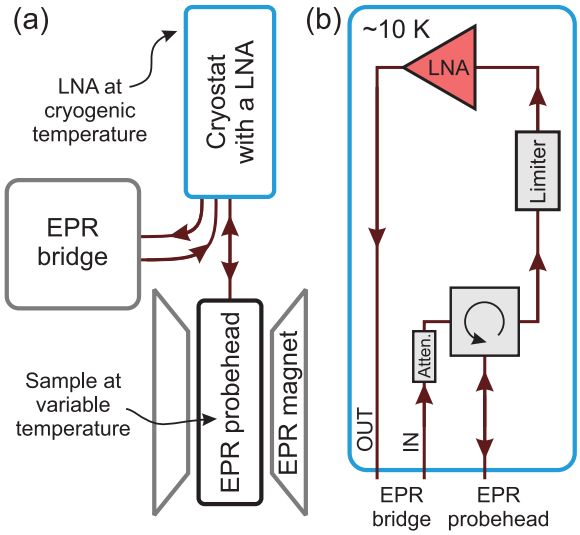

Fig. 3. (a) Block diagram of our cryoprobe EPR setup with an externally cooled cryogenic LNA. (b) Schematic of the microwave circuit within the external cryostat, which is connected to the microwave bridge and EPR probehead. In practice, all microwave components are closely packed on a cold finger of the cryostat.

Table 1
Microwave components used for X- and Q-band EPR cryoprobes.

Component	X-band	Q-band
LNA	LNF LNC4_16B (36 dB gain, 4 K noise temperature at 4 K and 9.5 GHz)	LNF LNC28_52WB (34 dB gain, 9 K noise temperature at 4 K and 34 GHz)
Limiter	Narda-MITEQ LIM301 (500 W peak power, 130 mW flat leakage, $<$ 200 ns recovery time, 0.1% duty cycle)	Pasternack PE80L2002 (20 W peak power, 63 mW flat leakage, 10 ns recovery time, 0.1% duty cycle)
Circulator	Pasternack PE83CR000	Pasternack PE83CR1032

pler, where a fraction of signal power (25% for a 6 dB coupling) is lost to the coupled port. In addition, a circulator does not suppress the input microwave power allowing higher bandwidth pulses. However, as demonstrated in our previous work and in the theoretical analysis presented above, attenuation at the input is actually necessary to obtain the best SNR, as it also suppresses the thermal noise from the source [12]. In the current setup, to test the suppression of this noise, we use easily-interchangeable cryogenic attenuators attached to the input port of the circulator (Fig. 3b).

In contrast to our previous design [12], here we also no longer use a fast microwave switch to additionally protect the LNA, as our testing showed that the LNA is capable of handling flat leakage power of the limiter making the switch redundant although a slow degradation of the performance may still occur. Absence of the microwave switch also makes the CW operation and tuning of the resonator easily accessible.

We also note that the external cryostat has input and output ports that should be connected to the EPR bridge, while typical commercial X-band spectrometers are designed to operate only in the reflection mode and thus have only one microwave port. We solve this problem by bypassing the internal circulator in the microwave bridge, which is a simple modification. A more elegant solution would be to exploit the intermediate frequency (IF) mode, which is available on X-band Bruker spectrometers having an IF extension, although we have not thoroughly tested this approach.

3.2. Q-band

We use the same setup design at Q-band, which is based on a high-frequency Low Noise Factory LNC28_52WB amplifier (Table 1) placed in the external cryostat together with its protection circuit (Fig. 3). The amplifier is protected by a fast Pasternack PE80L2002 limiter (Table 1) from high power pulses originating from a 10 W solid state amplifier. The components are interconnected by low loss 2.92 mm type coaxial cables, while we use coaxial-to-waveguide WR-28 adapters (Pastnernack PE9826) to interconnect cables and waveguides. The cryoprobe is connected to a Q-band EPR probehead (EN5107D2) placed in an Oxford Instruments CF935 cryostat, which allows us to perform the CW and pulsed EPR/ENDOR experiments at different sample temperature. The output of the cryoprobe is directly connected to the detection path of the IF-Q module of our microwave bridge bypassing the internal circulator.

4. Experimental details

4.1. Pulsed EPR experiments

To benchmark our setup at X-band, we used a standard coal sample placed in a 4 mm outer diameter EPR tube, which was inserted into the fully overcoupled ER4118X-MD5 resonator. The SNR improvement was characterized using a Hahn echo pulse sequence ($\pi/2 - \tau - \pi - \tau -$ echo) with two-step phase cycling. The echo was integrated to obtain the echo-detected field sweep (EDFS) spectra and echo decay curves of the same sample. For measurements using no additional input attenuation, the duration of the π pulse was 40 ns, while for attenuation of 20 dB, the pulse length was increased to 160 ns. To avoid saturation of the digitizer, the interpulse delay τ was adjusted to produce a sufficiently weak echo signal. Depending on the sample temperature, the shot repetition time was chosen sufficiently long to avoid saturation of the signal.

The SNR improvement and its uncertainty were determined using at least 10 separate measurements of the Hahn echo. The traces were corrected by subtracting constant backgrounds, which proved to be almost negligible. The intensity of the spin signal was taken as a maximum of the echo obtained by fitting a Gaussian peak function, while noise was calculated as the standard deviation of the signal far away from the echo (at least 500 data points were used for noise calculation).

Pulsed EPR experiments at Q-band were performed using the IF-Q option of our spectrometer equipped with the fully overcoupled EN5107D2 Q-band probehead and 10 W AmpQ-10 solid state amplifier. For these experiments, we placed a small amount of the coal sample in a 1.6 mm outer diameter EPR tube, and the SNR improvement was quantified following the same procedure as described above. The π pulse duration was 40 ns for 0 dB input attenuation, while it was increased to 100 ns for 18 dB attenuation.

During all experiments, the sample position and resonator coupling were tightly fixed to avoid potential variations when switching between both setups. All parameters, except for the microwave power and negligible changes in the microwave frequency and magnetic field, were kept constant in both measurements. The microwave power from the bridge was adjusted to yield the same duration of the π pulse in both setups, i.e. to achieve the same microwave power at the EPR resonator.

4.2. Pulsed ENDOR experiments

We performed Pulsed ENDOR experiments using a Bruker DICE ENDOR system equipped with a 150 W radiofrequency amplifier. Measurements at X- and Q-band were performed on the same coal sample placed in 4 mm and 1.6 mm outer diameter EPR tubes, which were inserted into the fully overcoupled EN4118X-MD4 and EN5107D2 EPR probeheads, respectively. We used the Mims pulse sequence [17] with the microwave pulse length of $\pi/2$ = 20 ns, while the radiofrequency π pulse was set to 10 μs. The interpulse delay τ between the microwave pulses was adjusted to yield a weak echo signal and was 306 ns (X-band) and 1.5 μs (Q-band). For SNR improvement calculation, the ENDOR spectra were baseline corrected and normalized to the spin signal, while noise was determined by calculating the standard deviation of signal far away from the ENDOR lines.

4.3. CW experiments

We used the same coal samples to benchmark the SNR improvement for the CW EPR experiments at both frequency bands. For measurements at X-band, the high-Q ER4102ST resonator was used with the modulation field of 2 G and 100 kHz. The Q-band CW EPR experiments were performed using the

EN5107D2 resonator and 2 G and 50 kHz modulation field. The resonators were critically coupled for the CW EPR measurements. The SNR improvement was calculated by comparing the noise levels after baseline correction and normalization of the spectra.

5. Results and discussion

5.1. SNR improvement at different temperature

We investigated the performance of our setups by measuring the Hahn echo of the standard coal sample and comparing it to the unmodified spectrometer. Fig. 4 shows the comparison of the echoes obtained with the cryoprobes and unmodified setups, when the samples were held at $T_S = 10$ K temperature. At X-band, the sensitivity improvement can be observed with a corresponding increase of voltage SNR close to 4×. Due to the additional noise and losses of the current setup, the sensitivity gain is about two times lower compared to the previous design at $T_S = 10$ K, where the microwave components were placed directly on the EPR probehead [12]. The voltage SNR improvement at Q-band is lower compared to the X-band setup, but still reaches a significant factor of about 2.2×.

We investigated how the sample temperature affects the sensitivity improvement provided by our setups by performing the same type of Hahn echo experiments on the coal sample. The obtained results are presented in Fig. 5a demonstrating sensitivity gain independent of T_S for both frequency bands in sharp contrast to our previous setup [12], where the SNR improvement gradually diminished with increasing sample/LNA temperature. For comparison, the current X-band setup enhances SNR by 3.7× at $T_S = 294$ K, while the previous cryoprobe resulted in substantially lower improvement of about 2× at the same sample temperature.

We also measured the echo-detected field sweep (EDFS) spectra of the same samples at room temperature by integrating the Hahn echo. The obtained spectra at each band are presented in Fig. 6 revealing similar SNR improvements as obtained from the Hahn echo experiments (Fig. 5a). More importantly, these experiments show that the lineshapes are not affected by our cryoprobe setups indicating no saturation effects for signals of moderate intensity.

We also investigated the SNR improvement at different LNA (cryoprobe) temperatures T_{LNA}, when the sample was kept at room temperature. The obtained results are presented in Fig. 5b revealing a decrease of the SNR gain at both frequency bands as the cryoprobe temperature is increased to room temperature. At X-band, the decrease is from 3.7× to 2.3×, while Q-band experiments show a loss of the SNR improvement from 2.2× to about 1×. Such a degradation of sensitivity mainly occurs due to a significant increase of the noise temperatures of the amplifiers and other microwave components. For example, the X-band LNA at 4 K and 294 K has noise temperature of 4 K and 50 K, respectively, while the Q-band amplifier has higher noise temperatures (9 K and 125 K).

We note that even with the LNA at room temperature, a significant SNR gain of 2.3× can be achieved at X-band, which can be attributed to lower losses in our microwave circuit and better noise characteristics of the LNA compared to the unmodified Bruker spectrometer. We observed a similar enhancement using our previous setup at room temperature [12] suggesting that higher microwave losses inevitably introduced by much longer microwave path of the current setup are compensated by the absence

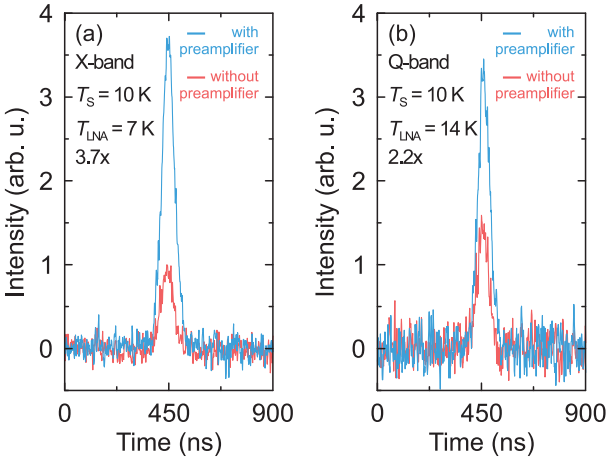

Fig. 4. Hahn echoes of the coal sample obtained at 10 K using (a) X- and (b) Q-band setups with and without the cryoprobe with the corresponding voltage SNR improvements of (a) 3.7× and (b) 2.2×. The echoes are normalized to the noise level. The LNAs were cooled down to the lowest accessible temperatures. Experimental parameters: (a) $\tau = 2$ μs, 4 averages, $t_\pi = 40$ ns, and (b) $\tau = 5$ μs, 1 average, $t_\pi = 40$ ns. In both cases, the attenuator on the input path was absent (0 dB).

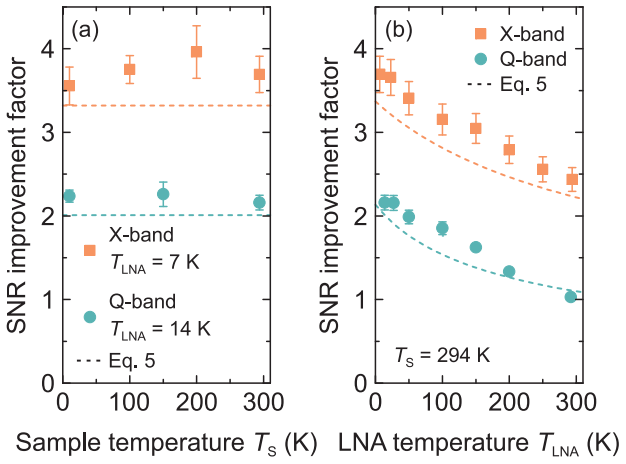

Fig. 5. SNR improvement provided by our X- and Q-band cryoprobes for different (a) sample and (b) LNA temperatures. The dashed curves show calculated SNR improvement using Eq. 5. In all cases, the attenuator on the input path was absent (0 dB).

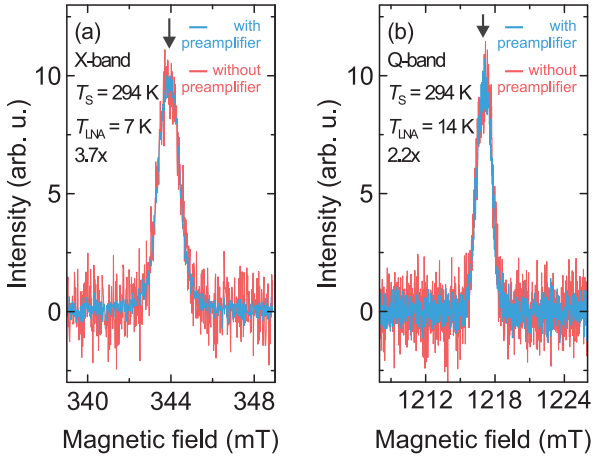

Fig. 6. Normalized EDFS spectra of the coal sample obtained at (a) X- and (b) Q-band setups with and without the cryoprobe with the corresponding voltage SNR improvements of (a) 3.7× and (b) 2.2×. The sample temperature was 296 K. Experimental parameters: (a) $\tau = 0.5$ μs, 4 averages, $t_\pi = 40$ ns, and (b) $\tau = 2.5$ μs, 2 averages, $t_\pi = 40$ ns. In both cases, the attenuator on the input path was absent (0 dB). The arrows indicate the fields, at which the Hahn echo experiments were performed.

of the microwave switch and employment of a circulator instead of a directional coupler. Cooling the LNA in our current setup enhances the SNR by a further factor of 1.7×.

We measured the microwave losses of our setups (see Figure S2) and used Eq. 5 to compare the experimentally obtained SNR improvement with our theoretical model. Assuming no suppression of the input thermal noise ($T_{in}^{C} = 294$ K), the calculated improvements are about 10% lower than the experimental values (3.3× (X-band) and 2.0× (Q-band)) showing a good agreement with the experiment (see Fig. 5a). A small discrepancy may originate from uncertainties in the measurements of the microwave losses or from a slight suppression of the input thermal noise by cold circulators and microwave cables in the cryoprobe, which does not fully recover in the room temperature microwave path interfacing the cryoprobe and the EPR resonator. By assuming $T_{in}^{C} \sim 220$ K, we recover a good agreement with the experimental results for both frequency bands.

Our theoretical framework also allow us to estimate how the SNR improvement is affected by the temperature of the cryoprobe at both frequency bands. For our calculations, we assumed that the LNA noise temperature depends linearly on the physical temperature of the amplifier T_{LNA}. The obtained results are presented in Fig. 5b demonstrating a good agreement with the experimental data.

We investigated the effect of the input thermal noise suppression on the SNR improvement in more detail by placing different cryogenic attenuators on the input path (see Fig. 3b), while keeping the sample at room temperature. We observed that at X-band the SNR improvement increased from 3.7× to about 4.4× for 5 dB input attenuation and then saturated for higher levels of attenuation (see Fig. 7). For Q-band setup, the increase was marginal from 2.2× (0 dB) to about 2.4× (18 dB). These results indicate a partial suppression of the input thermal noise (lowering of T_{in}^{C}), even when the sample is held at room temperature, although rather small improvements suggest that the input thermal noise cannot be fully suppressed in both systems due to the presence of the microwave paths at room temperature after the cryoattenuators.

5.2. Pulsed ENDOR

In contrast to our previous design [12], the current cryoprobe poses no restrictions to utilize more bulky ENDOR probeheads allowing us to characterize the SNR improvement for X- and Q-band ENDOR experiments. Fig. 8 shows the room temperature ENDOR spectra of the same coal samples obtained using our cryoprobe with 0 dB input attenuation together with the spectra measured using unmodified spectrometers. The obtained voltage SNR improvement is 3.9× (X-band) and 2.1× (Q-band) in a good agreement with the Hahn echo and EDFS experiments indicating full compatibility of our current design with the ENDOR experiments.

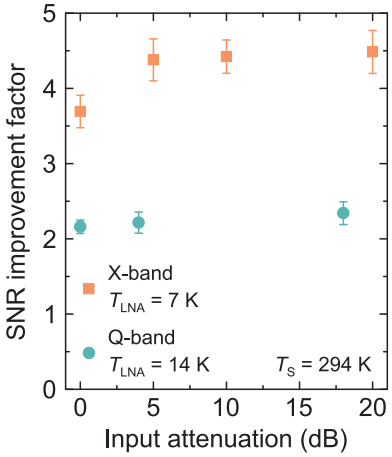

Fig. 7. SNR improvement vs. input attenuation provided by our X- and Q-band cryoprobes. The sample temperature was 294 K, while the LNAs were cooled down to the lowest accessible temperatures.

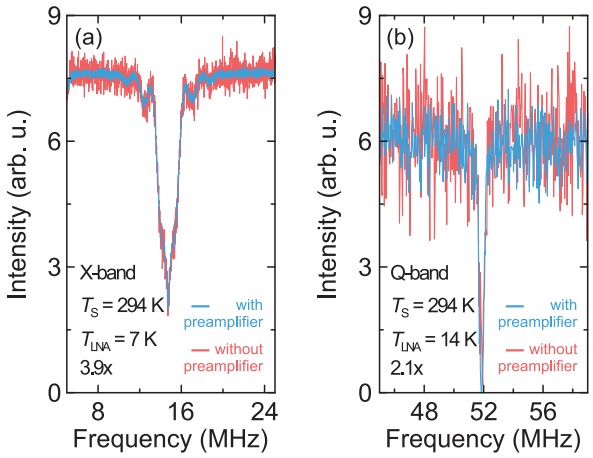

Fig. 8. Normalized ^{1}H Mims ENDOR spectra of the coal sample obtained at (a) X- and (b) Q-band setups with and without the cryoprobe with the corresponding voltage SNR improvements of (a) 3.9× and (b) 2.1×. The sample temperature was 296 K. Experimental parameters: (a) τ = 306 ns, 10 averages, t_π = 40 ns, t_{rf} = 10 μs, and (b) τ = 1.5 μs, 1 average, t_π = 40 ns, t_{rf} = 8 μs. In both cases, the attenuator on the input path was absent (0 dB).

5.3. CW

We also tested the performance of our setups for the CW EPR experiments at both frequency bands. Fig. 9 shows the room temperature CW EPR spectra of the coal samples obtained with and without the cryoprobe. The determined SNR enhancement is 3.2× and 2.0× at X- and Q-band, respectively, demonstrating compatibility of our setups with the CW EPR experiments despite a slightly worse performance compared with the pulsed EPR results. A lower value of the SNR improvement may result from additional noise introduced by the microwave source, which is present during

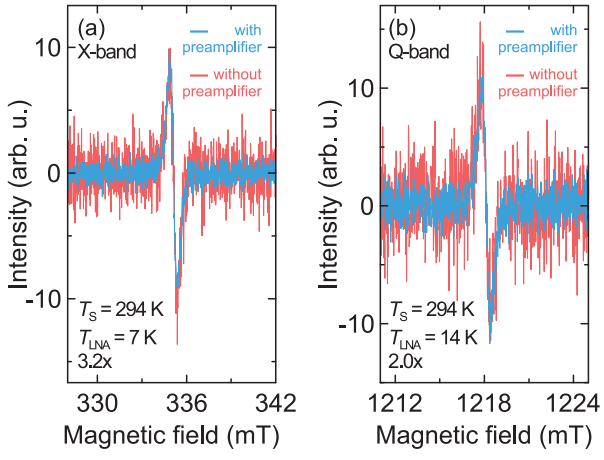

Fig. 9. Normalized CW EPR spectra of the coal sample obtained at (a) X- and (b) Q-band with and without the cryoprobe with the corresponding voltage SNR improvements of (a) 3.2× and (b) 2.0×. The sample temperature was 296 K. Experimental parameters: (a) 0.15 μW, 1 average, modulation field: 2 G and 100 kHz, and (b) 0.016 μW, 1 average, modulation field: 2 G and 50 kHz. In both cases, the attenuator on the input path was absent (0 dB).

the signal acquisition [8]. We note that here the experiments at X-band were performed using a high-Q TE_{102} rectangular cavity, which cannot be directly equipped with a cryogenically cooled LNA, as the sample cryostat is placed within the resonator itself, making our current cryoprobe design the only feasible solution for such EPR resonators.

5.4. Limitations and further improvements

Our calculations show that to further improve the performance of our setups it is essential to minimize losses of the room temperature microwave path joining the cryoprobe and EPR probehead. Cooling this interface would be also beneficial, as, in addition to smaller noise temperature, this would provide a better suppression of the input thermal noise. Such a setup would correspond to the third cryoprobe design presented in Fig. 2d, which, however, is much more difficult to realise in practise. We note that reduction of the microwave losses of the cold components prior the LNA would also increase the sensitivity of our cryoprobe, although the effect would be rather small, as the highest contributors to the effective noise temperature are the room temperature microwave paths.

As a shortcoming of both our cryoprobe setups, we observed a deviation of the signal from the expected exponential decay during a Hahn echo decay experiment at short values of τ ($\lesssim$180 ns) (Figure S3), which may be critical for very fast relaxing spin species. Observation of this effect at both frequency bands suggests that it is not related to the recovery of the limiters, as the Q-band limiter has very fast recovery time of 10 ns. A plausible explanation for this discrepancy might be saturation of the LNAs by leaking microwave pulses, as the flat leakage of the limiters is higher than the maximum specified CW power of the LNAs. We also tested different configurations of the protection circuit of the X-band setup, for example, by replacing the circulator with a directional coupler, but the issue remained, although we observed that the discrepancy is somewhat sensitive to different assemblies and in some cases it is very small.

Other limitations of the X-band setup related to the limiter recovery and LNA saturation by strong spin signals are described in our previous work [12], therefore here we concentrate on the Q-band case. The 1 dB compression point (CW) of the employed Q-band LNA is 0.1 mW meaning that it may saturate for very strong signals. Indeed, we observed some clipping of the echoes, but only when the signal amplitude was close to saturation of the digitizer. This shows that the dynamic range of the Q-band setup is wide enough for the majority of EPR samples. The saturation of the LNA also puts a limit to the microwave power used during mode tuning and CW EPR experiments, and care should be taken not to exceed this power level to avoid damaging of the amplifier.

Another limitation of the Q-band setup is the peak power of the used limiter, which is only 20 W (Table 1). Such power levels are fully compatible with our solid state amplifier, but not with the state-of-the-art Q-band TWTs ($\sim$ 200 W), which are becoming more popular in the community [18]. This issue can be solved by replacing the limiter or using a fast switch to protect the LNA as mentioned in Ref. [18]. We also note that the used Q-band limiter has a duty cycle of 0.1% meaning that the shot repetition time should be carefully adjusted when using sequences with long microwave pulses.

6. Conclusions

In this work, we theoretically and experimentally explored a more general approach to the EPR cryoprobe, where the microwave amplifier temperature is decoupled from the sample temperature. Our experimental realisation of such X- and Q-band cryoprobe is based on a cryogenically cooled LNA situated in a separately cooled closed cycle He cryostat. In contrast to our previous design [12], this approach provides a moderate sensitivity gain even for room temperature experiments and is fully compatible with all CW and pulsed EPR/ENDOR resonators. The obtained gains in SNR can be used to reduce the spin concentration or sample volume allowing more advanced X- and Q-band EPR experiments (e.g. hyperfine [19] and dipolar [20–23], spectroscopies) with increased sensitivity.

We also discussed prospects of further sensitivity improvement of cryoprobe setup based on reduction of the microwave losses and suppression of the input thermal noise. Our simulations show that for the best performance it is essential to minimize the losses and cool down the microwave lines interfacing the resonator and the LNA. This should be feasible in closed cycle He cryostats, where a variable temperature insert (sample region) and a pulse tube (LNA region) are integrated into a single unit providing the ultimate EPR cryoprobe solution.

Data and materials availability

Data needed to evaluate the conclusions in the paper can be found at dx.doi.org/10.18279/MIDAS.SPECTR.203438. Additional data related to this paper may be requested from the authors.

Declaration of Competing Interest

The authors declare the following financial interests/personal relationships which may be considered as potential competing interests: [Mantas Simenas reports a relationship with Amplify My Probe Ltd. that includes: equity or stocks. Vidmantas Kalendra reports a relationship with Amplify My Probe Ltd. that includes: equity or stocks.]

Acknowledgement

The research reported in this publication was supported by funding from the European Union HORIZON-MSCA-2021-PF-01 Marie Skłodowska-Curie Fellowship (Project ID: 101064200; SPECTR, https://epr.ff.vu.lt/spectr) (M.Š., J.B.), and European Research Council (ERC) under the European Union's Horizon 2020 research and innovation programme (Grant agreement No. 771493) (J.J.L.M.). This work also received support from the Engineering and Physical Sciences Research Council (EP/W005794/1) (J.J.L.M.). We also thank Antoine Wolff from Bruker Corporation for the suggestion to use the IF mode to avoid bypassing of the internal circulator in the Bruker microwave bridge.

Appendix A. Supplementary material

Supplementary data associated with this article can be found, in the online version, at https://doi.org/10.1016/j.jmr.2022.107356.

References

[1] P. Styles, N. Soffe, C. Scott, D. Crag, F. Row, D. White, P. White, A high-resolution NMR probe in which the coil and preamplifier are cooled with liquid helium, J. Magn. Reson. 60 (1984) (1969) 397–404.
[2] P. Styles, N.F. Soffe, C.A. Scott, An improved cryogenically cooled probe for high-resolution NMR, J. Magn. Reson. 84 (1989) (1969) 376–378.
[3] L. Darrasse, J.-C. Ginefri, Perspectives with cryogenic RF probes in biomedical MRI, Biochimie 85 (2003) 915–937.
[4] H. Kovacs, D. Moskau, M. Spraul, Cryogenically cooled probes - a leap in NMR technology, Prog. Nucl. Magn. Reson. Spectrosc. 46 (2005) 131–155.
[5] W.J. Wallace, R.H. Silsbee, Microstrip resonators for electron-spin resonance, Rev. Sci. Instrum. 62 (1991) 1754–1766.

[6] H.E. Altink, T. Gregorkiewicz, C.A.J. Ammerlaan, Sensitive electron paramagnetic resonance spectrometer for studying defects in semiconductors, Rev. Sci. Instrum. 63 (1992) 5742–5749.
[7] S. Pfenninger, W. Froncisz, J. Hyde, Noise analysis of EPR spectrometers with cryogenic microwave preamplifiers, J. Magn. Reson., Ser. A 113 (1995) 32–39.
[8] G.A. Rinard, R.W. Quine, R. Song, G.R. Eaton, S.S. Eaton, Absolute EPR spin echo and noise intensities, J. Magn. Reson. 140 (1999) 69–83.
[9] S. Vasilyev, J. Järvinen, E. Tjukanoff, A. Kharitonov, S. Jaakkola, Cryogenic 2 mm wave electron spin resonance spectrometer with application to atomic hydrogen gas below 100 mK, Rev. Sci. Instrum. 75 (2004) 94–98.
[10] R. Narkowicz, H. Ogata, E. Reijerse, D. Suter, A cryogenic receiver for EPR, J. Magn. Reson. 237 (2013) 79–84.
[11] Y. Artzi, Y. Twig, A. Blank, Induction-detection electron spin resonance with spin sensitivity of a few tens of spins, Appl. Phys. Lett. 106 (2015) 084104.
[12] M. Šimėnas, J. O'Sullivan, C.W. Zollitsch, O. Kennedy, M. Seif-Eddine, I. Ritsch, M. Hülsmann, M. Qi, A. Godt, M.M. Roessler, G. Jeschke, J.J. Morton, A sensitivity leap for X-band EPR using a probehead with a cryogenic preamplifier, J. Magn. Reson. 322 (2021) 106876.
[13] K.H. Richardson, J.J. Wright, M. Šimėnas, J. Thiemann, A.M. Esteves, G. McGuire, W.K. Myers, J.J.L. Morton, M. Hippler, M.M. Nowaczyk, G.T. Hanke, M.M. Roessler, Functional basis of electron transport within photosynthetic complex I, Nat. Commun. 12 (2021) 5387.
[14] J. O'Sullivan, O.W. Kennedy, C.W. Zollitsch, M. Šimėnas, C.N. Thomas, L.V. Abdurakhimov, S. Withington, J.J. Morton, Spin-Resonance Linewidths of Bismuth Donors in Silicon Coupled to Planar Microresonators, Phys. Rev. Appl. 14 (2020) 064050.
[15] M. Simenas, J. O'Sullivan, O.W. Kennedy, S. Lin, S. Fearn, C.W. Zollitsch, G. Dold, T. Schmitt, P. Schüffelgen, R.-B. Liu, J.J.L. Morton, Near-Surface $^{125}Te^{+}$ Spins with Millisecond Coherence Lifetime, Phys. Rev. Lett. 129 (2022) 117701.
[16] H. Friis, Noise figures of radio receivers, Proc. IRE 32 (1944) 419–422.
[17] W.B. Mims, Pulsed Endor Experiments, Proc. R. Soc. London, Ser. A 283 (1965) 452–457.
[18] Y. Polyhach, E. Bordignon, R. Tschaggelar, S. Gandra, A. Godt, G. Jeschke, High sensitivity and versatility of the DEER experiment on nitroxide radical pairs at Q-band frequencies, Phys. Chem. Chem. Phys. 14 (2012) 10762–10773.
[19] P. Höfer, A. Grupp, H. Nebenführ, M. Mehring, Hyperfine sublevel correlation (hyscore) spectroscopy: a 2D ESR investigation of the squaric acid radical, Chem. Phys. Lett. 132 (1986) 279–282.
[20] M. Pannier, S. Veit, A. Godt, G. Jeschke, H. Spiess, Dead-time free measurement of dipole-dipole interactions between electron spins, J. Magn. Reson. 142 (2000) 331–340.
[21] G. Jeschke, M. Pannier, A. Godt, H. Spiess, Dipolar spectroscopy and spin alignment in electron paramagnetic resonance, Chem. Phys. Lett. 331 (2000) 243–252.
[22] P.P. Borbat, J.H. Freed, Multiple-quantum ESR and distance measurements, Chem. Phys. Lett. 313 (1999) 145–154.
[23] S. Milikisyants, F. Scarpelli, M.G. Finiguerra, M. Ubbink, M. Huber, A pulsed EPR method to determine distances between paramagnetic centers with strong spectral anisotropy and radicals: The dead-time free RIDME sequence, J. Magn. Reson. 201 (2009) 48–56.